Asian Journal of Chemistry; Vol. 37, No. 7 (2025), 1803-1812

ASIAN JOURNAL OF CHEMISTRY

https://doi.org/10.14233/ajchem.2025.33917

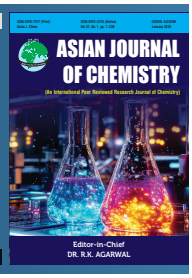

Theoretical and Biological Evaluations of Vanadyl, Cobalt and Copper Chelates: DFT, Molecular Docking and Antimicrobial Investigations

SHEETAL[1], PRAVEEN KUMAR GUPTA[1,*], SELVA KUMAR RAMASAMY[1], AMIT KUMAR[2,*], RAMAN KUMAR[3] and SONU SHARMA[3]

[1]Department of Chemistry, Maharishi Markandeshwar (Deemed to be University), Mullana-133207, India
[2]Department of Chemistry, Indira Gandhi National College, Ladwa, Kurukshetra-136132, India
[3]Department of Bio-Sciences and Technology, Maharishi Markandeshwar (Deemed to be University), Mullana-133207, India

*Corresponding authors: E-mail: parveen.gupta@mmumullana.org; amitvash76@gmail.com

Received: 25 April 2025; *Accepted*: 28 June 2025; *Published online*: 30 June 2025; AJC-22057

New biologically active complexes of VO^{IV}, Co^{II} and Cu^{II} were synthesized and characterized by CHNS, FTIR, mass, magnetic susceptibility, DRS and EPR techniques. The ligand precursor was synthesized by the reaction between *o*-phenylenediammine and thiophene-2-carbaldehyde, which was subsequently coordinated with metal ions (VO^{IV}, Co^{II} and Cu^{II}) to synthesize the complexes with the general formula $[M(C_{32}H_{24}N_4S_4)]X_2$ [M = VO^{IV}, Co^{II} and Cu^{II}; X = Cl, SO_4^{2-}]. The coordination process followed a 2:1 (ligand-to-metal) stoichiometry for VO(IV), Co(II) and Cu(II) complexes. Structural analysis suggested a square pyramidal geometry for vanadium, an octahedral arrangement for cobalt and a square planar configuration for copper. Additionally, DFT-based computational methods were performed to evaluate key quantum chemical parameters and some biological descriptors of the ligand and its metal complexes. The antibacterial screening against *E. coli*, *S. aureus*, *B. subtilis* and *P. aeruginosa* showed that all the metal complexes displayed significantly enhanced antimicrobial activity compared to the uncoordinated ligand. To gain further insight into protein-ligand interactions, *in silico* docking analyses were performed and the ADME study was used to confirm their drug-like properties, reinforcing their potential as bioactive agents.

Keywords: Metal complex, Schiff base, Antimicrobial study, DFT, Docking study.

INTRODUCTION

Designing new Schiff base ligand precursors has gained significant interest in recent years owing to their versatile structures and diverse physico-chemical properties [1]. Their ability to act as stabilizing agents makes them valuable in the synthesis of metal complexes across different oxidation states. Their structural flexibility and ability to form stable metal complexes with *d*-block elements make them privileged and ideal ligands to study in coordination chemistry [2]. Schiff base ligands when incorporated with hetero atoms like N, O and S effectively produce a effective coordination environment, significantly influencing the chemistry and reactivity of associated metal complexes [3]. Moreover, the multidentate nature of ligands also ensures chelation, which often leads to enhanced stability and unique structural properties in the resulting metal complexes [4]. This metal-ligand interaction also controls and enhances the biological, chemical and electrochemical activities of the metal centres [3,5]. The presence of both N and O donor atoms and halogen groups in Schiff base metal complexes enhances their appeal due to their promising antibacterial properties [6]. It is widely recognized that the coordination of these ligands with metal ions can greatly enhance their antibacterial effectiveness [7]. Schiff bases represent an important category of bioactive compounds that have attracted considerable attention from medicinal and pharmaceutical chemists because of their diverse pharmacological activities [8,9] such as antiviral [10], anticancer [11,12], antibacterial [13], antioxidant [14], antifungal [15], anticonvulsant [16], antidiabetic [17], anti-inflammatory [18], *etc*. Despite that Schiff bases are also utilized in catalysis [19], designing molecular magnets [20], solvent extraction of different metal ions [21] and optical and membrane sensors [22,23]. The latest research also highlights that Schiff base metal complexes with Cu(II), Co(II) and VO(IV) demonstrate significantly better antibacterial performance, against diverse bacterial strains [24-31].

To combat the emerging microbial infectious diseases, there is a strong need for the development of novel antimicrobial scaffolds. In this context and keeping in view the medicinal and other applications, new copper(II), cobalt(II) and vanadium(IV) complexes containing *o*-phenylenediammine and 2-thiophene carboxyaldehyde moieties have been synthesized and characterized. The antibacterial potential of these metal complexes were evaluated against selected bacterial strains. DFT methods were employed to determine the geometric structures of the ligand and its corresponding metal complexes. Molecular docking simulations were also performed to predict atomic-level interactions between a ligand molecule and a known target protein, offering insights into small molecule binding behaviour at protein active sites and elucidating essential biochemical processes.

EXPERIMENTAL

Chemicals *o*-phenylenediammine and 2-thiophenecarboxyaldehyde were purchased from Aldrich. The metal salts like copper(II) chloride, cobalt(II) chloride hexahydrate, vanadyl sulfate and the solvents *viz*. ethanol, methanol, hexane and ethylacetate were procured from CDH and used as such. The purity of Schiff base ligand was assessed through thin-layer chromatography analysis. A mixture of pure hexane and ethyl acetate was used as a solvent for TLC and column chromatography. The infrared spectral data were recorded over the range of 400-4000 cm^{-1} on a Shimadzu IR Spirit Fourier transform infrared spectrometer. Diffuse reflectance spectra (DRS) were obtained by utilizing a Shimadzu UV-2600 double-beam spectrophotometer in the 200-1200 nm range with $BaSO_4$ as standard. CHNS analysis was conducted using a Thermo-Scientific Flash 2000 instrument. The vanadium content was determined using the gravimetric approach, while the back titration method was employed for assessing the metal content in the copper and cobalt complex. Electron spin resonance (ESR) spectra of vanadyl and manganese complexes were performed at room temperature on a JES FA200 instrument.

Synthesis of ligand precursor: The Schff base ligand was synthesized by condensation of *o*-phenylenediammine and 2-thiophene carboxaldehyde. An ethanolic solution of 2-thiophene carboxaldehyde (2.24 g, 20 mmol) was slowly added to an ethanolic solution of *o*-phenylenediamine (1.08 g, 10 mmol) (**Scheme-I**). The reaction mixture was subjected to reflux for 30 h. The resulting yellowish-brown solution was concentrated by evaporation and subsequently cooled in an ice bath. The yellow-brown precipitate formed was isolated by filtration, washed multiple times with hot ethanol followed by methanol MeOH and then dried in an oven. The purity of the ligand was preliminarily observed by applying TLC (ethyl acetate: hexane 2:8).

Synthesis of metal complexes: The metal complexes were synthesized following an identical procedure (**Scheme-II**). An ethanolic solution of the respective metal salt (5 mmol) was added dropwise to a vigorously stirred ethanolic Schiff base ligand solution (5 mmol). The resulting mixture was refluxed for 1-2 h in a water bath and then allowed to cool. Coloured precipitates of the metal complexes formed, which were collected by filtration, washed thoroughly with hot ethanol followed by methanol and then dried in an oven at 80 ºC.

***In vitro* antibacterial study:** The antibacterial properties of Schiff base ligand and its corresponding metal complexes were evaluated utilizing the agar well diffusion assay. This involved testing against two Gram-positive bacterial strains, *S. aureus* and *B. subtilis*, along with two Gram-negative strains, *E. coli* and *P. aeruginosa*. To perform the assay, agar plates were inoculated with bacterial cultures and wells of approximately 6-8 mm in diameter were punched using sterilized cork borers. A fixed concentration of the test compounds dissolved in DMSO was then added into each well. Following incubation at 37 ºC for a designated duration, the antimicrobial efficacy was determined by measuring the inhibition zone diameters around the wells, expressed in millimeters. The antimicrobial performance of the synthesized metal complexes was assessed relative to the standard antibiotics such as ciprofloxacin and cephalosporin.

DFT calculations: Computational analyses were conducted using the GAUSSIAN 09 software [32], with molecular structures visualized through GaussView. The optimization of ground-state geometries was carried out using theoretical analysis conducted through DFT employing the B3LYP hybrid functional, utilizing the 6-311G (d,p) basis set 6-311G (d,p) for elements (C, H, N, O and S) and the LanL2DZ effective core potential was applied for transition metals such as Co, Cu and V [33]. To verify that the structures correspond to global minima, optimizations ensured the absence of negative vibrational frequencies. The solvent environment was incorporated through the conductor like polarizable continuum model within both DFT and TD-DFT calculations. In addition, Gauss Sum

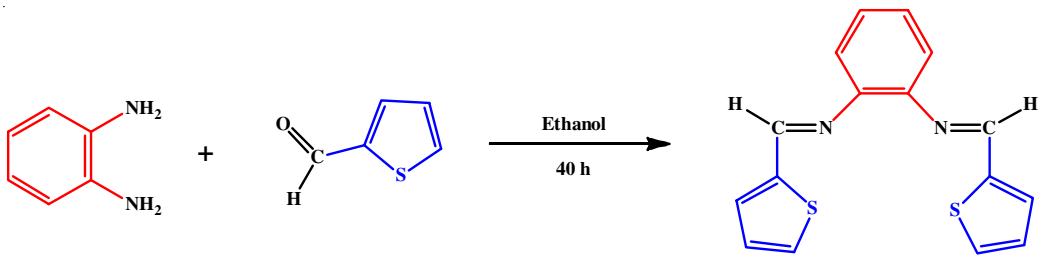

***N*,*N'*-(1,2-Phenylene)-*bis*(1-(thiophen-2-yl)methanimine) (2TH-OPDA)**

Scheme-I: Synthetic route of ligand (2TH-OPDA)

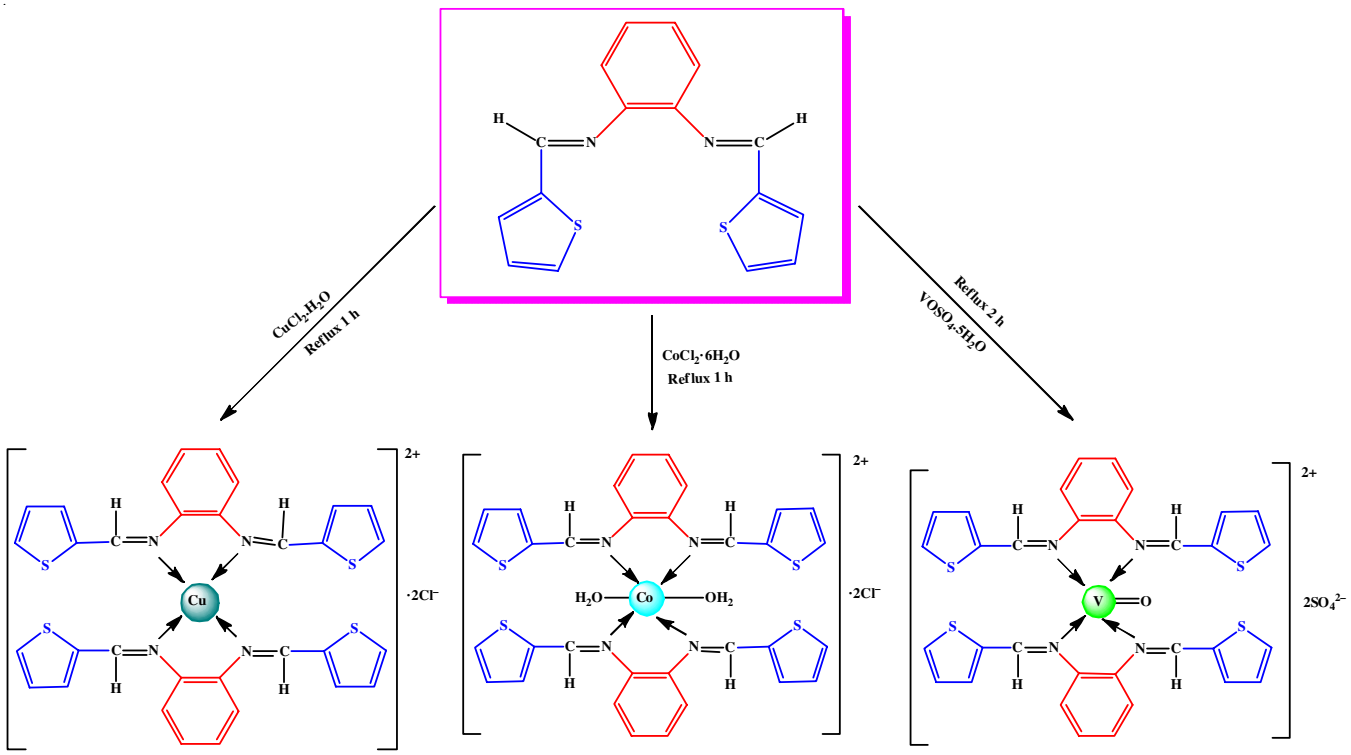

Scheme-II: Preparation of Cu^{2+}, Cu^{2+} and VO^{4+} complexes

[34] was employed to determine the fractional contributions of molecular orbitals from different atomic groups, while the spectral analysis was performed using Chemissian [35].

Molecular docking: Molecular docking simulations for the lead compounds were conducted using AutoDock4 [36], employing the Lamarckian genetic algorithm to determine binding strength across multiple conformations. AutoDock Tools (ADT) was employed to carry out docking protocols and related computational tasks. Crystal structures of bacterial targets, including DNA gyrase B (1KZN) and thymidylate kinase (4QGG), were collected from the Protein Data Bank (https://www.rcsb.org/), were utilized with a resolution of 1.90 Å to explore the antimicrobial potential of the ligand and its corresponding metal complexes [37]. During protein preparation, water molecules were removed to prevent unintended interactions with the docked conformers. Molecular interactions were examined and displayed in 2D and 3D formats with the aid of BIOVIA Discovery Studio 2016 [38].

RESULTS AND DISCUSSION

The ligand precursor was synthesized by refluxing a 1:2 molar ratio of *o*-phenylenediammine and 2-thiophene carboxaldehyde in absolute ethanol (**Scheme-I**). Synthesis of the Cu^{2+}, Co^{2+} and VO^{4+} complexes was achieved using an equimolar (1:1) ratio of metal ion to ligand, as outlined in **Scheme-II**. The ligand shows solubility in methanol and warm ethanol, while both the free ligand and its metal complexes are soluble in solvents such as DMF and DMSO. Table-1 summarizes their physical parameters and analytical findings.

^{1}H NMR and infrared spectra: The ligand was analyzed by NMR spectroscopy in DMSO-d_6 at room temperature (Fig. 1). The peaks at δ 3.36 ppm were attributed to DMSO H_2O protons. The peaks in the range δ 5.9-7.8 ppm correspond to 12 protons due to four phenyl protons, six thiophene protons and two azomethine hydrogen. The key IR spectral profiles of the ligand and its corresponding metal complexes are tabulated in Table-2. The IR spectrum of the ligand displays a prominent peak at 1581 cm^{-1}, corresponding to C=N stretching, which undergoes a shift of 15-30 cm^{-1} in the metal complexes. This spectral shift indicates the coordination of the azomethine nitrogen to the metal ions (Fig. 2). Furthermore, a band at 844 cm^{-1}, attributed to the C–S stretching vibration of the thiophene group, remains largely unchanged in the complexes, indicating that the sulfur atom remains non-coordinated [39]. The involvement of the azomethine nitrogen in metal ion coordination is additionally supported by the appearance of metal-nitrogen bands

TABLE-1
PHYSICO-CHEMICAL CHARACTERIZATION OF THE LIGAND AND ITS CORRESPONDING METAL COMPLEXES

Compounds (m.f.)	Colour	Elemental analysis (%): Calcd. (Found)				
		C	H	N	S	M
2TH-OPDA ($C_{16}H_{12}N_2S_2$)	Brownish-yellow	64.84 (64.80)	4.08 (4.02)	9.45 (9.39)	21.63 (21.58)	–
2TH-OPDA-Cu ($C_{32}H_{24}Cl_2N_4S_4Cu$)	Light green	52.85 (52.80)	3.33 (3.26)	7.70 (7.60)	17.63 (17.57)	8.74 (8.71)
2TH-OPDA-Co ($C_{32}H_{28}Cl_2N_4O_2SCo$)	Sky blue	45.12 (45.09)	2.84 (2.77)	6.58 (6.53)	22.58 (22.47)	5.98 (5.92)
2TH-OPDA-V ($C_{32}H_{24}N_4O_9S_6V$)	Dark green	49.43 (49.34)	3.27 (3.12)	6.99 (6.92)	23.99 (23.92)	6.35 (6.27)

TABLE-2
ELECTRONIC AND INFRARED SPECTRAL PROFILE OF LIGAND AND COMPLEXES

Ligand/complexes	Infrared (cm^{-1})				Electronic data		Magnetic moment (B.M)
	ν(C=N)	ν(C-S)	ν(M-N)	ν(V=O)	λ_{max} (cm^{-1})	Transitions	
2TH-OPDA	1581	844	–	–	38314, 29940	$\pi\rightarrow\pi^*$; $n\rightarrow\pi^*$	–
2TH-OPDA-Cu	1564	841	540	–	15083	$^2B_{1g}\rightarrow{}^2A_{1g}$, $^2B_{1g}\rightarrow{}^2B_{2g}$, $^2B_{1g}\rightarrow{}^2E_g$	1.80
2TH-OPDA-Co	1566	844	549	–	8764, 12987, 18518	$^4T_{1g}\rightarrow{}^4T_{2g}(F)$; $^4T_{1g}\rightarrow{}^4A_{2g}(F)$ $^4T_{1g}\rightarrow{}^4T_{1g}(P)$	3.94
2TH-OPDA-V	1551	843	534	973	12180, 16129, 22988	$^2B_2\rightarrow{}^2E$, $^2B_2\rightarrow{}^2B_1$; $^2B_2\rightarrow{}^2A_1$	1.76

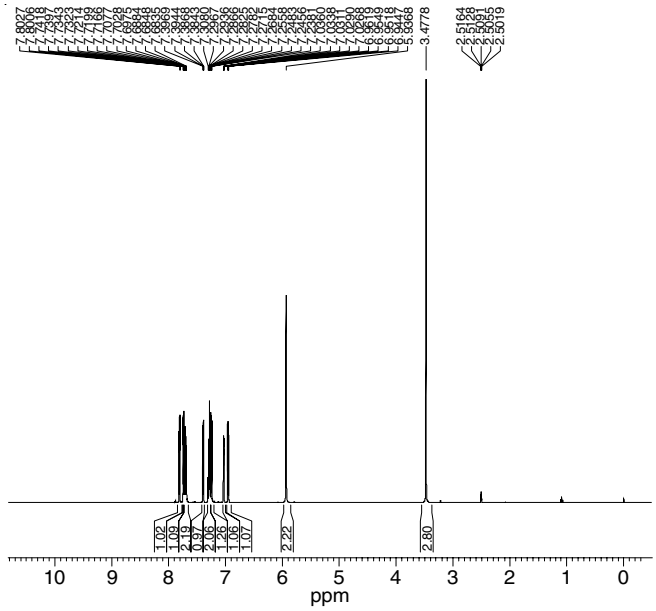

Fig. 1. ^1H NMR spectra of ligand

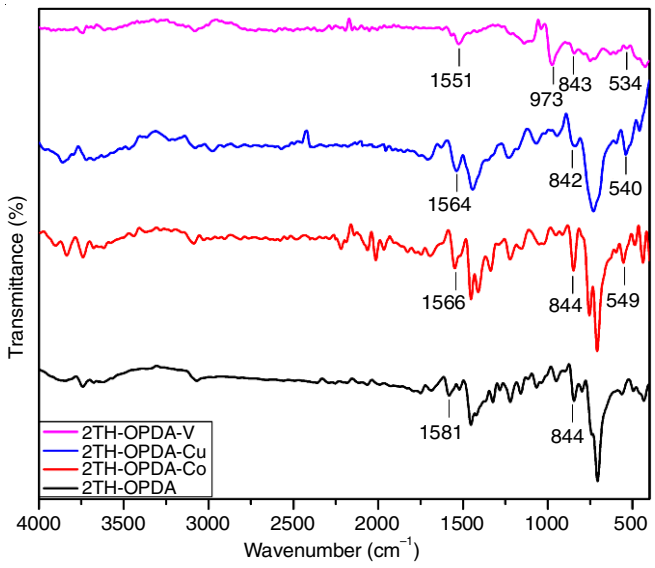

Fig. 2. IR spectra of ligand and its metal complexes

at 540 cm^{-1}, 549 cm^{-1} and 534 cm^{-1} in the Cu^{2+}, Co^{2+} and VO^{4+} complexes, respectively. Notably, the vanadyl complex reveals a characteristic sharp peak at 973 cm^{-1} (V=O) stretching vibration [40].

Electronic and magnetic study: The electronic profile of the Schiff base ligand and its corresponding metal complexes are represented in Fig. 3. The electronic spectra of the Schiff

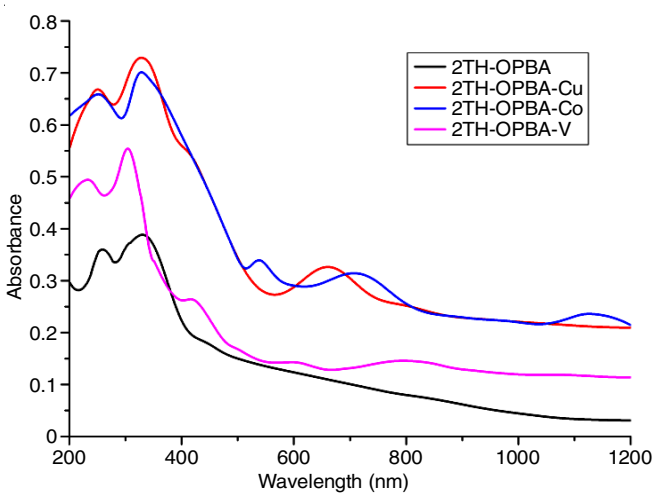

Fig. 3. Electronic spectra of ligand and its metal complexes

base ligand displayed distinct peaks at 38314 and 29940 cm^{-1}, corresponding to $\pi\rightarrow\pi^*$ and $n\rightarrow\pi^*$ transitions. These bands experienced small shifts as a result of coordination with metal ions (Table-2). In case of the copper complex, a broad envelope of characteristic d→d electronic transitions was observed at 15083 cm^{-1}, which was due to the combination of three ligand field transitions $^2B_{1g}\rightarrow{}^2A_{1g}$ $^2B_{1g}\rightarrow{}^2B_{2g}$ and $^2B_{1g}\rightarrow{}^2E_g$ [41]. Moreover, the magnetic moment value of 1.80 B.M. for the Cu(II) complex is consistent with a square planar geometry. In contrast, the Co(II) complex displayed absorption bands at 8764, 12987 and 18518 cm^{-1}, corresponding to $^4T_{1g}(F)\rightarrow{}^4T_{2g}(F)$, $^4T_{1g}(F)\rightarrow{}^4A_{2g}(F)$ and $^4T_{1g}(F)\rightarrow{}^4T_{1g}(P)$ transitions, respectively [42] confirming its octahedral geometry, which was further supported by a magnetic moment of 3.94 B.M. The vanadium complex exhibited three distinct *d-d* transitions $^2B_{2g}\rightarrow{}^2E_g$, $^2B_{2g}\rightarrow{}^2B_{1g}$ and $^2B_{2g}\rightarrow{}^2A_{1g}$ in the spectral range of 12180, 16129 and 22988 cm^{-1}, indicative of a square pyramidal coordination environment [43], which is consistent with the experimental magnetic moment value of 1.76 B.M.

Mass spectral study: Fig. 4a-c displays the mass spectra of the synthesized metal complexes displaying the molecular ion peaks that closely match the calculated values, confirming their compositions. For [2TH-OPDA-Cu], a molecular ion signal was observed at *m/z* 656.99, corresponding to $[C_{32}H_{24}CuN_4S_4]^+$, validating its structure. Similarly, the cobalt complex [2TH-OPDA-Co] exhibited a molecular ion signal at *m/z* 687.96, attributed to $[C_{32}H_{28}CoN_4O_2S_4]^+$, confirming its formation. Similarly, vanadium complex [2TH-OPDA-V] displayed a signal at *m/z* 658.99, corresponding to $[C_{32}H_{24}N_4OS_2V]^+$, further supporting its structural identity.

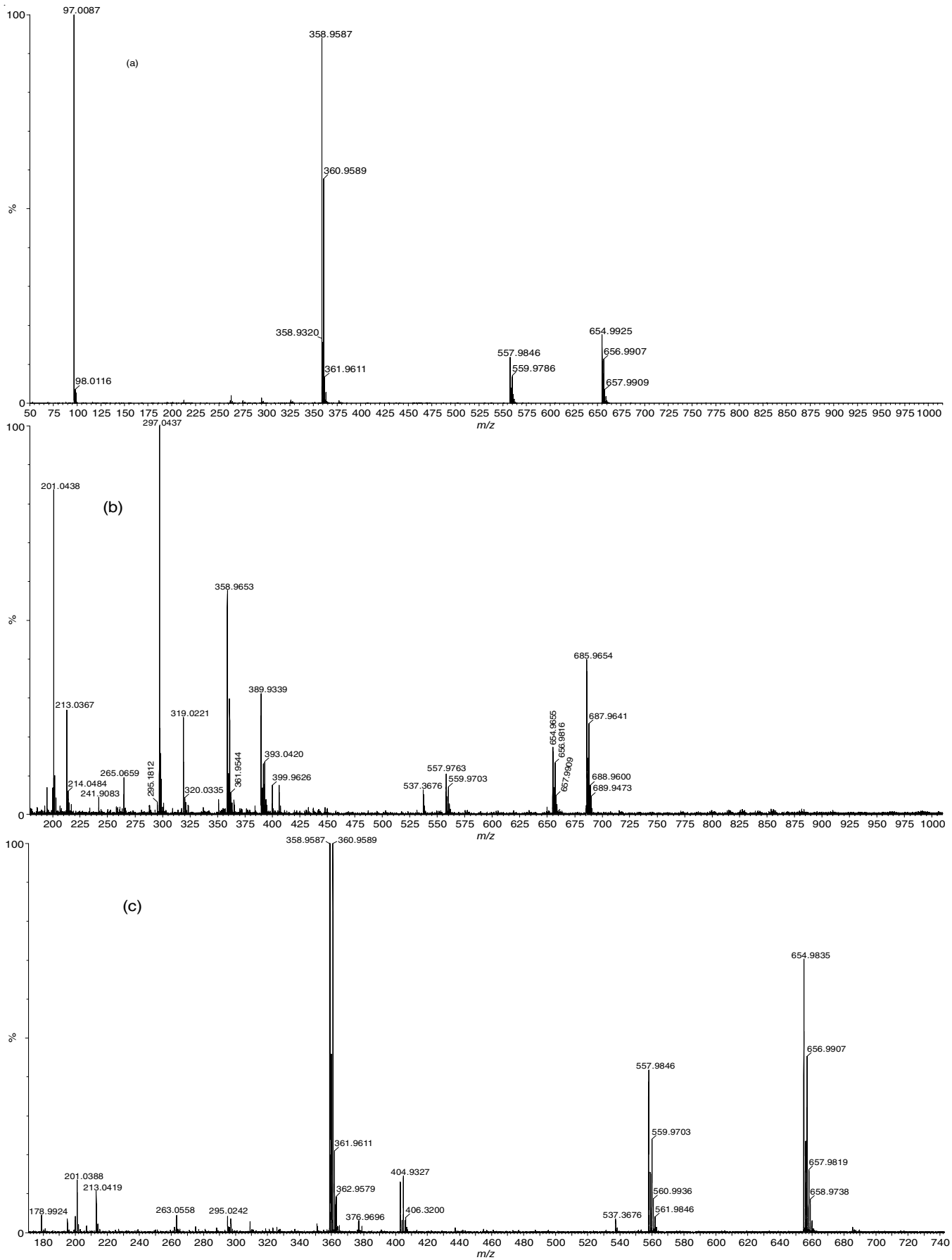

Fig. 4. Mass spectra of (a) copper complex, (b) cobalt complex and (c) vanadium complex

TABLE-3
ANTIMICROBIAL POTENTIAL OF THE LIGAND AND ITS COMPLEXES WITH MINIMUM INHIBITORY ZONES (mm)

Conc. (µL)	Inhibition zone (mm)															
	2TH-OPDA				2TH-OPD-Cu				2TH-OPD-Co				2TH-OPD-V			
	E.c.	*B.s.*	*S.a.*	*P.a.*	*E.c.*	*B.s.*	*S.a.*	*P.a.*	*E.c.*	*B.s.*	*S.a.*	*P.a.*	*E.c.*	*B.s.*	*S.a.*	*P.a.*
5	–	–	–	–	–	–	–	–	–	–	–	–	–	–	–	–
10	–	–	–	–	11	0	13	11	11	0	13	0	10	0	0	0
20	–	–	–	–	12	12	14	12	12	10	14	0	11	0	11	0
40	–	–	–	–	12	13	14	13	13	11	14	0	11	0	12	12
80	10	11	10	–	13	15	14	14	13	12	14	10	12	0	13	12
100	11	11	11	–	13	15	15	16	13	13	15	12	13	18	17	13
250	11	11	12	–	14	15	15	18	15	14	15	14	14	19	18	13
500	12	12	12	–	20	15	15	20	17	15	15	15	17	21	21	15

E.c. = E. coli; *B.s. = B. subtilis*; *S.a. = S. aureus*; *P.a. = P. aeruginosa*

EPR spectra: Fig. 5 presents the ESR spectra of vanadium and copper complexes at ambient temperature. The copper(II) complex exhibits a distinct four-line pattern due to hyperfine coupling with the Cu nucleus (I = 3/2), showing significant anisotropy and suggesting a distorted octahedral geometry (g = 2.16, A = 74 G) [44]. The vanadyl complex displays a well-resolved eight-line pattern from hyperfine coupling with the VO nucleus (I = 7/2), with spin-Hamiltonian values (g = 1.99, A = 150 G) characteristic of VO^{2+} in a square pyramidal geometry [45]. These spectra confirm the paramagnetic oxidation states of VO(IV) and Cu(II). ESR parameters for the cobalt(II) complex could not be determined due to low-resolution splitting.

Biological activities: The antibacterial assessment of the synthesized metal complexes was evaluated using *E. coli*, *B. subtilis*, *S. aureus* and *P. aeruginosa*, with inhibition zones measured and compared to standard antibiotics, ciprofloxacin and cephalosporin (Tables 3 and 4). The control antibiotics exhibited strong inhibition, with ciprofloxacin showing zones of 22.25-28.37 mm and cephalosporin 24.01-27.74 mm, confirming their high efficacy. Among the tested complexes, copper(II) complex demonstrated moderate antibacterial activity, with inhibition increasing at higher concentrations, reaching 20 mm for *E. coli* and *P. aeruginosa* at 500 µL. The cobalt(II) complex showed similar trends but with slightly lower potency, achieving a maximum inhibition of 21 mm for *P. aeruginosa*. The vanadyl complex exhibited the least antibacterial effect, with inhibition zones ranging from 12 mm at lower concentrations to 21 mm for *E. coli* at 500 µL. A comparative analysis revealed that while the copper and cobalt complexes displayed significant activity, particularly at higher concentrations, they remained less effective than the reference drug. These results suggest that although these metal complexes do not match the potency of conventional antibiotics, they hold potential as alternative antimicrobial agents, especially when used at elevated concentrations. The enhanced potential of metal complexes can be attributed to chelation, which reduces metal ion polarity and increases interaction with bacterial cells.

TABLE-4
ZONE INHIBITION (mm) OF ANTIMICROBIAL POTENTIAL OF CONTROL (ANTIBIOTIC)

Control	*E. coli*	*B. subtilis*	*S. aureus*	*P. aeruginosa*
Ciprofloxacin	28.37	25.07	22.25	28.32
Cephalosporin	27.74	26.97	24.01	27.55

DFT study: Theoretical calculations based on DFT were conducted to analyze the electronic properties and molecular stability of the synthesized ligand and its corresponding complexes. The calculations were performed using the B3LYP functional and the B3LYP/6-31G**/LanL2DZ ECP basis set to

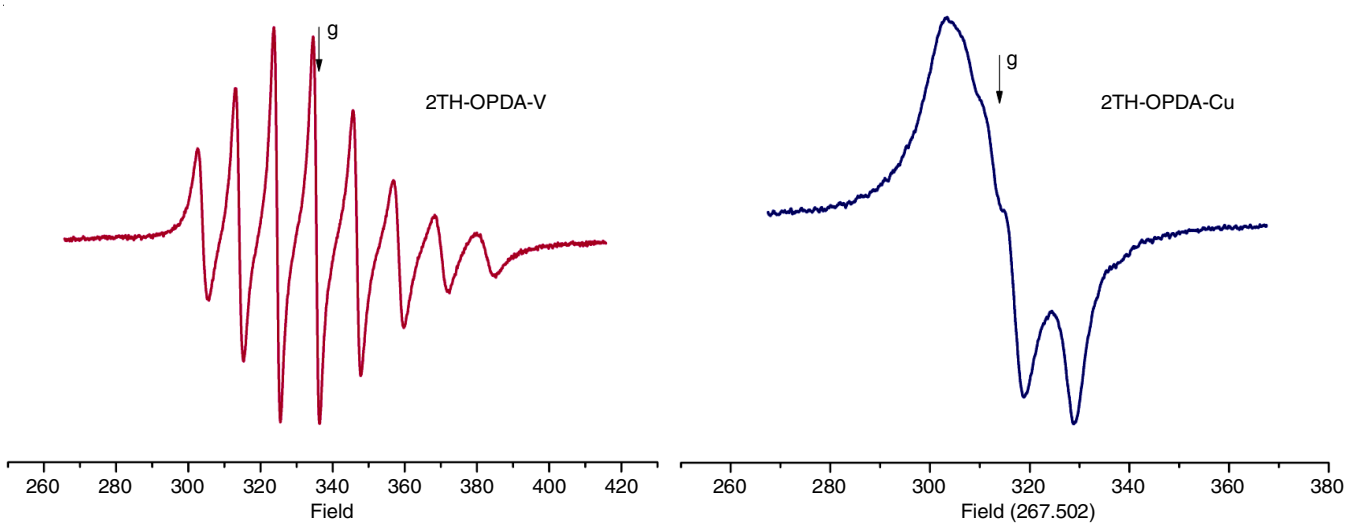

Fig. 5. Room temperature X-band EPR spectra of vanadium and copper complex

determine optimized geometries, frontier orbital energies and other quantum chemical parameters. The optimized structures and molecular orbitals are demonstrated in Fig. 6, while the key electronic parameters are summarized in Table-5.

The ΔE value, representing the HOMO-LUMO energy gap, plays an essential role in predicting the chemical reactivity and stability of the molecules. The free ligand exhibited a ΔE of 4.21 eV, whereas metal coordination significantly reduced this gap, enhancing charge transfer potential. Among the metal complexes, the copper(II) complex displayed the lowest energy gap (2.48 eV), suggesting higher reactivity and better electron delocalization, followed by vanadyl (2.79 eV) and cobalt (2.28 eV). The dipole moment of the copper(II) complex was also significantly higher (8.85 D), indicating enhanced polarity, which may contribute to better solubility and interaction with biological targets. Several quantum chemical descriptors were determined based on the expressions provided in eqns. 1-5. The electrophilicity index (ω), a key descriptor for biological activity, was found to be highest for the vanadyl complex (-20.69), followed by cobalt (-17.09) and copper (-12.86), suggesting their potential for strong biomolecular interactions. Theoretical results support the antibacterial activity findings, supporting the role of electronic properties in biological activity.

$$\chi = -\frac{1}{2}(E_{HOMO} + E_{LUMO}) \quad (1)$$

$$\mu = -\chi = \frac{1}{2}(E_{HOMO} + E_{LUMO}) \quad (2)$$

$$\eta = \frac{1}{2}(E_{HOMO} - E_{LUMO}) \quad (3)$$

$$S = \frac{1}{2\eta} \quad (4)$$

$$\omega = \frac{\mu^2}{2\eta} \quad (5)$$

Docking studies: Docking studies were carried out to evaluate the binding interactions between the Schiff base ligand and its metal complexes with bacterial thymidylate kinase (PDB: 4QGG) and DNA gyrase B (PDB: 1KZN), both of which are crucial for bacterial survival. The binding affinities and key docking parameters are summarized in Table-6. The docking results suggests that metal coordination enhanced the binding affinity of the ligand, with the copper complex exhibiting the highest binding energy (-7.19 kcal/mol) against DNA gyrase

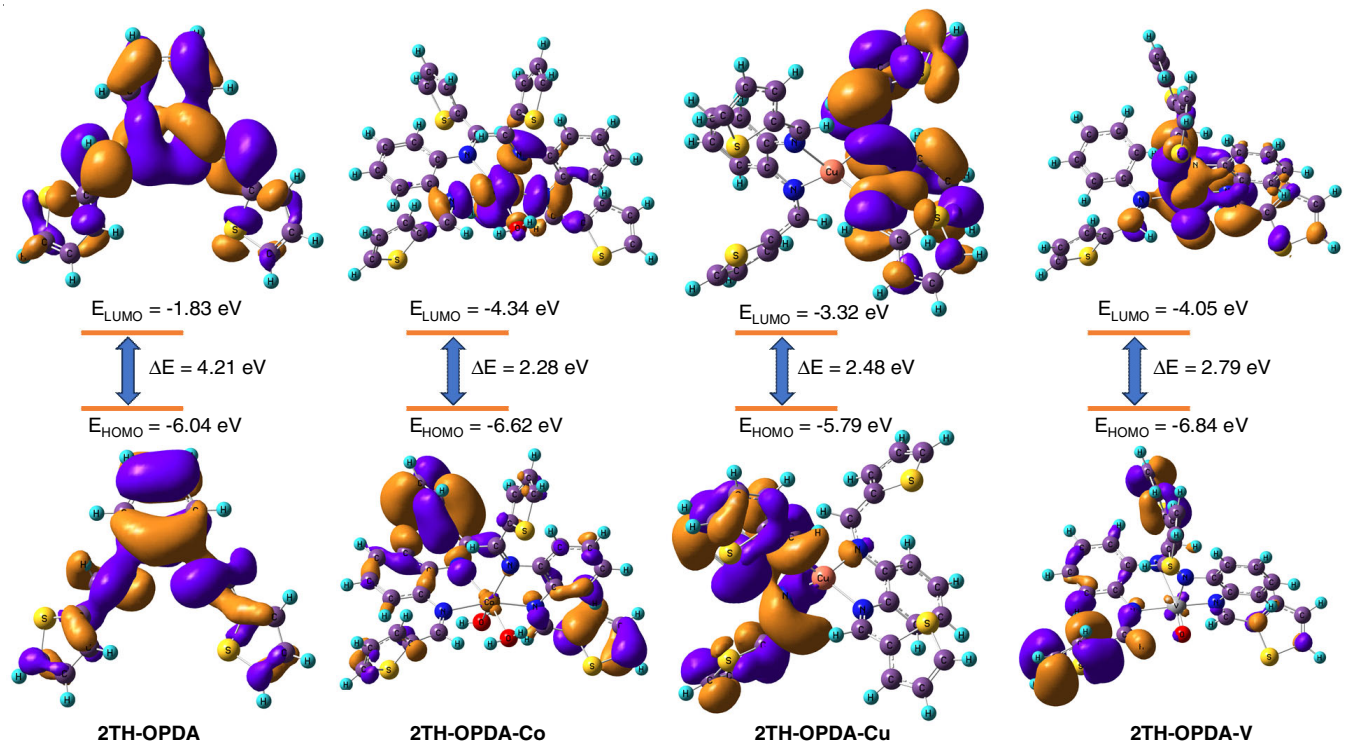

Fig. 6. Ground state optimized geometry and FMOs of Schiff base and its complexes by DFT/B3LYP method

TABLE-5
CALCULATIONS FOR DFT MOLECULAR ORBITAL ENERGIES

Compd.	Energy	DM	HOMO	LUMO	Gap	χ	?	η	S	ω
2TH-OPDA	-959338.33	1.57	-6.04	-1.83	-4.21	3.94	-3.94	-2.10	-1.05	-16.31
2TH-OPDA-Co	-2106151.80	0.64	-6.62	-4.34	-2.28	5.48	-5.48	-1.14	-0.57	-17.09
2TH-OPDA-Cu	-2041634.47	8.85	-5.79	-3.32	-2.48	4.56	-4.56	-1.24	-0.62	-12.86
2TH-OPDA-V	-2010843.65	4.03	-6.84	-4.05	-2.79	5.44	-5.44	-1.40	-0.70	-20.69

DM = Dipole moment, ΔE = energy band gap, EH = energy of HOMO, EL = energy of LUMO, η = global hardness, μ = chemical potential, χ = electronegativity. S = global softness and ω = global electrophilicity index.

TABLE-6
DOCKING STUDIES OF LIGAND AND ITS COMPLEXES WITH BACTERIAL DNA GYRASE B AND THYMIDYLATE KINASE

Compounds	$(\Delta G_{binding})^{\alpha}$ (binding free energy)	$(\Delta G_{vdW + hb + desolv})$ (vdw_hb_desolv energy)	ΔG_{elec} (electrostatic energy)	ΔG_{total} (total internal energy)	ΔG_{tor} (torsional free energy)	ΔG_{unb} (unbound system energy)
Bacterial DNA gyrase B [1KZN]						
2TH-OPDA	-5.88	-7.0	-0.07	-0.98	1.19	-0.98
2TH-OPDA-Co	-5.43	-6.59	-0.03	-1.51	1.19	-1.51
2TH-OPDA-Cu	-7.19	-8.37	-0.01	-1.70	1.19	-1.70
2TH-OPDA-V	-6.05	-7.19	-0.05	-2.03	-1.19	-2.03
Thymidylate kinase [4QGG]						
2TH-OPDA	-4.25	-5.41	-0.03	-0.95	1.19	-0.95
2TH-OPDA-Co	-4.93	-6.05	-0.07	-1.51	1.19	-1.51
2TH-OPDA-Cu	-5.59	-6.84	-0.06	-1.59	1.19	-1.59
2TH-OPDA-V	-4.86	-6.0	-0.05	-1.87	1.19	-1.87

B, followed by vanadyl (-6.05 kcal/mol) and cobalt (-5.43 kcal/mol). Similar trends were observed for thymidylate kinase, where the copper complex again demonstrated the best interaction (-5.59 kcal/mol), followed by vanadyl (-4.86 kcal/mol) and cobalt (-4.93 kcal/mol). The free ligand had the weakest binding in both cases, indicating that metal coordination improves the protein-ligand interactions.

The 3D docking interaction models illustrate the binding conformations of the Schiff base ligand and its complexes with the target proteins, while the 2D interaction maps (Fig. 7) highlight the hydrogen bonding and hydrophobic interactions responsible for the stability of the complexes within the binding site. Moreover, Fig. 8 provides a visualization of hydrogen bond interactions within the protein-ligand complex. The strong binding affinities of the copper and vanadyl complexes suggest their potential as inhibitors of bacterial enzymes, aligning with the antibacterial activity observed *in vitro*.

Overall, the DFT and docking findings contribute to a deeper comprehension of the electronic nature and bio-interactive potential of the synthesized metal complexes. The copper complex emerged as the most promising antimicrobial candidate due to its favourable electronic structure, strong binding affinity and enhanced antibacterial activity. Further modifications and in-depth pharmacokinetic studies could enhance its potential as a lead compound for novel antimicrobial agents.

Conclusion

This work reports the synthesis and characterization new Schiff base metal complexes of vanadyl, cobalt and copper using *o*-phenylenediamine and thiophene-2-carbaldehyde as ligand precursors. Structural analysis confirmed square pyramidal geometry for vanadyl, octahedral coordination for cobalt and a square planar configuration for copper. DFT studies revealed that metal coordination reduces the energy gap and enhances the charge transfer potential. The antibacterial evaluation demonstrated that all the metal complexes exhibited stronger antimicrobial effects than the ligand alone with the copper complex showing the highest inhibition against *E. coli* and *P. aeruginosa*. The cobalt complex also displayed notable antibacterial effects, whereas the vanadyl complex was the least effective. Molecular docking outcomes further supported these findings, indicating that the copper complex had the strongest binding affinity with

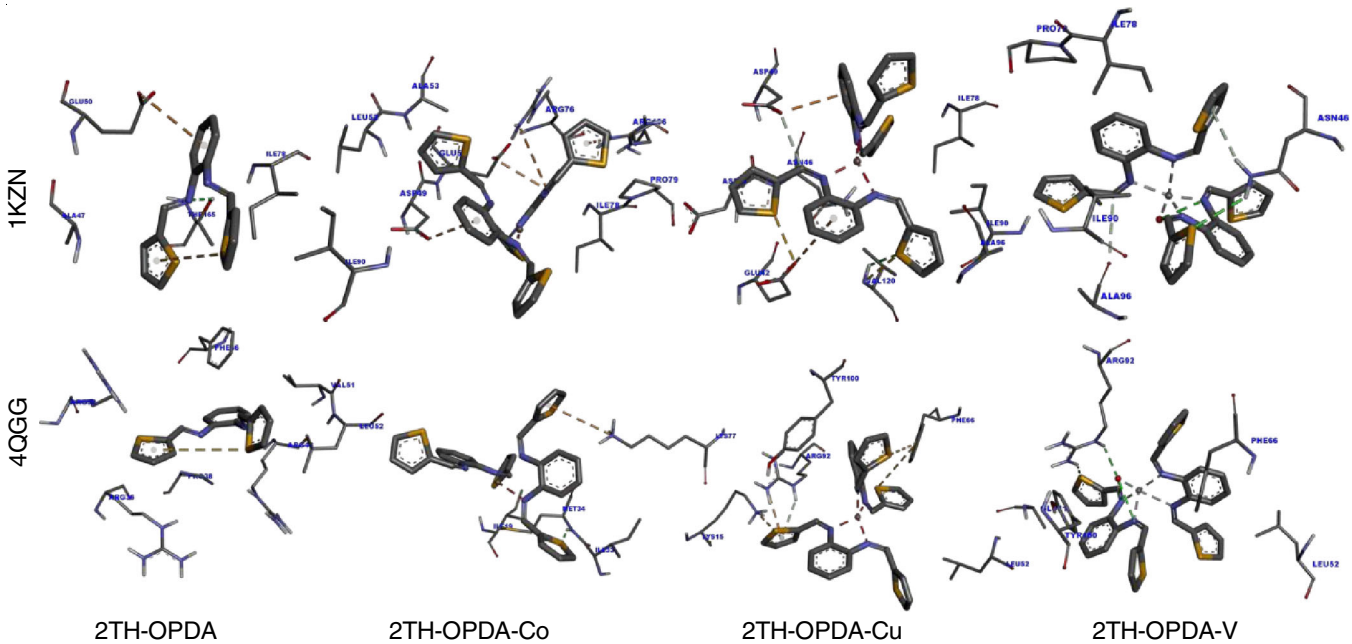

Fig. 7. Molecular docking 2D ligand interaction and its complexes with bacterial thymidylate kinase ad DNA gyrase B

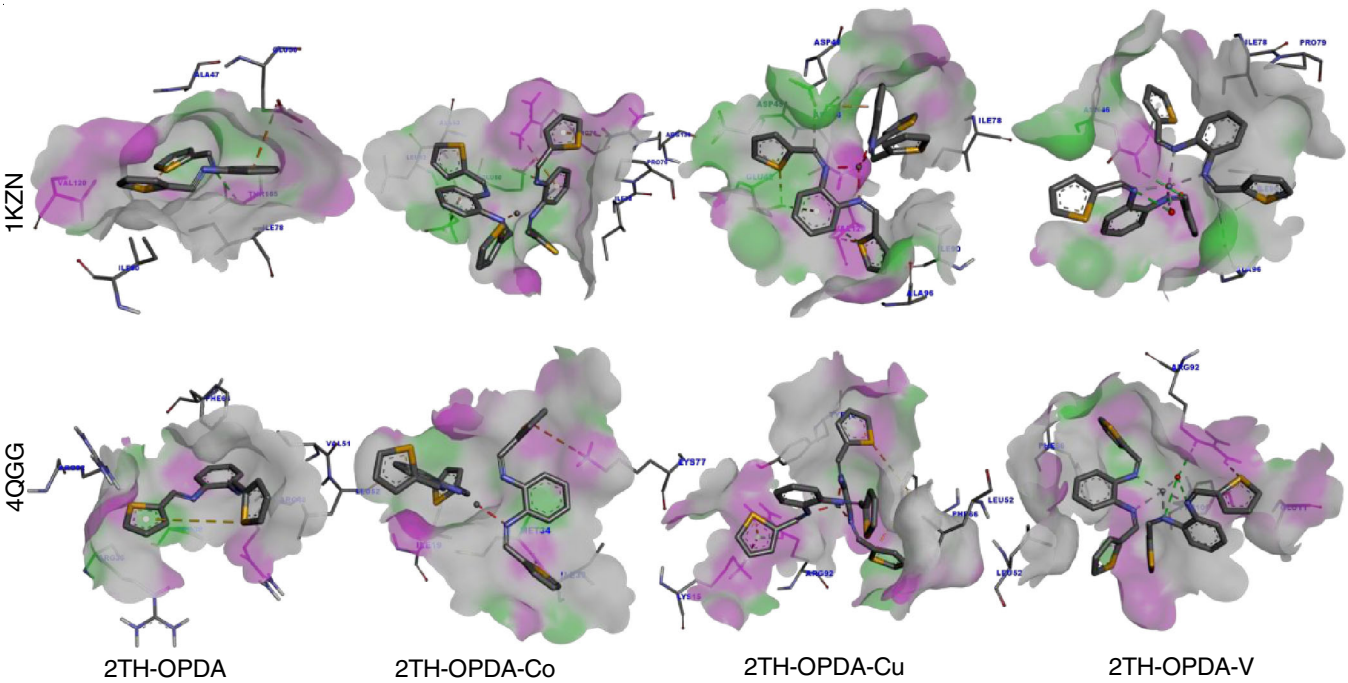

Fig. 8. Molecular docking hydrogen bonding interaction of Schiff base ligand and complexes with bacterial thymidylate kinase and DNA gyrase B

bacterial DNA gyrase B and thymidylate kinase, followed by vanadyl and cobalt complexes. Overall, the results suggest that metal complexation significantly enhances the biological activity of ligand. The copper complex, in particular, shows promise as a potential antimicrobial agent, with strong interactions at the molecular level and significant *in vitro* activity. Further, the structural modifications and pharmacokinetic evaluations could lead to the development of novel metal-based antimicrobial drugs.

ACKNOWLEDGEMENTS

The authors gratefully acknowledge to the Management of Maharishi Markandeshwar (Deemed to be University), Mullana, India, for its support and research facilities.

CONFLICT OF INTEREST

The authors declare that there is no conflict of interests regarding the publication of this article.

REFERENCES

1. C. Boulechfar, H. Ferkous, A. Delimi, A. Djedouani, A. Kahlouche, A. Boublia, A.S. Darwish, T. Lemaoui, R. Verma and Y. Benguerba, *Inorg. Chem. Commun.*, **150**, 110451 (2023); https://doi.org/10.1016/j.inoche.2023.110451
2. L. Lv, T. Zheng, L. Tang, Z. Wang and W. Liu, *Coord. Chem. Rev.*, **525**, 216327 (2025); https://doi.org/10.1016/j.ccr.2024.216327
3. D. Dinku, T.B. Demissie, I.N. Beas, R. Eswaramoorthy, B. Abdi and T. Desalegn, *Inorg. Chem. Commun.*, **160**, 111903 (2024); https://doi.org/10.1016/j.inoche.2023.111903
4. M. Kumar, A.K. Singh, S. Singh, A.K. Singh, P.K. Rao, R.K. Yadav, A.P. Singh and U.N. Tripathi, *J. Mol. Struct.*, **1319**, 139496 (2025); https://doi.org/10.1016/j.molstruc.2024.139496
5. P.R. Mandlik and P.R. Deshmukh, *Sch. Int. J. Chem. Mater. Sci.*, **7**, 190 (2024); https://doi.org/10.36348/sijcms.2024.v07i12.002
6. M. Aprajita and M. Choudhary, *Polyhedron*, **232**, 116296 (2023); https://doi.org/10.1016/j.poly.2023.116296
7. H.M.A. Al-Redha, S.H. Ali and S.S. Mohammed, *Baghdad Sci. J.*, **19**, 0704 (2022); https://doi.org/10.21123/bsj.2022.19.3.0704
8. S.K. Patil and B.T. Vibhute, *Arab. J. Chem.*, **14**, 103285 (2021); https://doi.org/10.1016/j.arabjc.2021.103285
9. S. Kaushik, S.K. Paliwal, M.R. Iyer and V.M. Patil, *Med. Chem. Res.*, **32**, 1063 (2023); https://doi.org/10.1007/s00044-023-03068-0
10. J. Zúñiga-Miranda, R. González-Pastor, S.E. Carrera-Pacheco, C. Rodríguez-Pólit, C. Barba-Ostria, A. Machado, L.P. Guamán, C.D. Alcivar-León and J. Heredia-Moya, *Discov. Appl. Sci.*, **7**, 115 (2025); https://doi.org/10.1007/s42452-025-06459-7
11. K.T. Tadele and T.W. Tsega, *Anticancer Agents Med. Chem.*, **19**, 1786 (2019); https://doi.org/10.2174/1871520619666190227171716
12. S. Kumar, S. Kumari, R. Karan, A. Kumar, R.K. Rawal and P.K. Gupta, *Inorg. Chem. Commun.*, **161**, 112014 (2024); https://doi.org/10.1016/j.inoche.2023.112014
13. P.Y. Chung, R.E.Y. Khoo, H.S. Liew and M.L. Low, *Ann. Clin. Microbiol. Antimicrob.*, **20**, 67 (2021); https://doi.org/10.1186/s12941-021-00473-4
14. F. Lemilemu, M. Bitew, T.B. Demissie, R. Eswaramoorthy and M. Endale, *BMC Chem.*, **15**, 67 (2021); https://doi.org/10.1186/s13065-021-00791-w
15. S. Mandal, A. Bhakat, S. Banerjee, K. Sarkar, D.B. Cordes, A.M.Z. Slawin and N.C. Saha, *J. Mol. Struct.*, **1313**, 138688 (2024); https://doi.org/10.1016/j.molstruc.2024.138688
16. R. Sahu and K. Shah, *Mini Rev. Med. Chem.*, **24**, 1632 (2024); https://doi.org/10.2174/0113895575302197240408121537
17. R. Sahu and K. Shah, *Curr. Pharm. Des.*, **31**, 37 (2025); https://doi.org/10.2174/0113816128339161240913055034
18. G.A. Krishna, T.M. Dhanya, A.A. Shanty, K.G. Raghu and P.V. Mohanan, *J. Mol. Struct.*, **1274**, 134384 (2023); https://doi.org/10.1016/j.molstruc.2022.134384
19. G. Balachandran, A. Dhamotharan, K. Kaliyamoorthy, K.S. Rajammal, R. Kulandaiya and A. Raja, *Eng. Proc.*, **61**, 26 (2024); https://doi.org/10.3390/engproc2024061026
20. S. Sepehrfar, M. Salehi, S. Parvarinezhad, A.M. Grzeœkiewicz and M. Kubicki, *J. Mol. Struct.*, **1278**, 134857 (2023); https://doi.org/10.1016/j.molstruc.2022.134857

21. M.F. Cheira, A.S. Orabi, M.A. Hassanin and S.M. Hassan, *Chem. Data Coll.*, **13-14**, 84 (2018); https://doi.org/10.1016/j.cdc.2018.01.003
22. A.L. Berhanu, Gaurav, I. Mohiuddin, A.K. Malik, J.S. Aulakh, V. Kumar and K.-H. Kim, *Trends Analyt. Chem.*, **116**, 74 (2019); https://doi.org/10.1016/j.trac.2019.04.025
23. W. Al Zoubi and N.D. Al Mohanna, *Spectrochim. Acta A Mol. Biomol. Spectrosc.*, **132**, 854 (2014); https://doi.org/10.1016/j.saa.2014.04.176
24. R.M. Rani and P. Kavitha, *Indian J. Chem.*, **63**, 281 (2024); https://doi.org/10.56042/ijc.v63i3.6539
25. S. Thakur, A. Jaryal and A. Bhalla, *Results Chem.*, **7**, 101350 (2024); https://doi.org/10.1016/j.rechem.2024.101350
26. J. Jorge, K.F. Del Pino Santos, F. Timóteo, R.R. Piva Vasconcelos, O. Ignacio Ayala Cáceres, I. Juliane Arantes Granja, D.M. de Souza, T.E. Allievi Frizon, G. Di Vaccari Botteselle, A. Luiz Braga, S. Saba, H. Rashid and J. Rafique, *Curr. Med. Chem.*, **31**, 2330 (2024); https://doi.org/10.2174/0929867330666230224092830
27. I.S. Turomsha, M.Y. Gvozdev, N.P. Osipovich, V.A. Staravoitava, D.I. Shiman and N.V. Loginova, *New J. Chem.*, **48**, 7134 (2024); https://doi.org/10.1039/D4NJ00430B
28. F.N. Ejiah, T.M. Fasina, N. Revaprasadu, F.T. Ogunsola and O.B. Familoni, *Lafia J. Sci. Ind. Res.*, **2**, 13 (2024); https://doi.org/10.62050/ljsir2024.v2n2.314
29. P. Durairaj, T. Maruthavanan, S. Manjunathan, S. Subashini, S.L. Rokhum and G. Baskar, *J. Mol. Struct.*, **1295**, 136650 (2024); https://doi.org/10.1016/j.molstruc.2023.136650
30. K. Hashmi, S. Satya, S. Gupta, A. Siddique, T. Khan and S. Joshi, *J. Trace Elem. Med. Biol.*, **79**, 127245 (2023); https://doi.org/10.1016/j.jtemb.2023.127245
31. J. Ceramella, D. Iacopetta, A. Catalano, F. Cirillo, R. Lappano and M.S. Sinicropi, *Antibiotics*, **11**, 191 (2022); https://doi.org/10.3390/antibiotics11020191
32. M.J. Frisch, G.W. Trucks, H.B. Schlegel, G.E. Scuseria, M.A. Robb, J.R. Cheeseman, G. Scalmani, V. Barone, B. Mennucci, G.A. Petersson, H. Nakatsuji, M. Aricato, X. Li, H.P. Hratchian, A.F. Izmaylov, J. Bloino, G. Zheng, J.L. Sonnenberg, M. Hada, M. Ehara, K. Toyota, R. Fukuda, J. Hasegawa, M. Ishida, T. Nakajima, Y. Honda, O. Kitao, H. Nakai, T. Vreven Jr., J.A. Montgomery, J.E. Peralta, F. Ogliaro, M. Bearpark, J.J. Heyd, E. Brothers, K.N. Kudin, V.N. Staroverov, R. Kobayashi, J. Normand, K. Raghavachari, A. Rendell, J.C. Burant, S.S. Iyengar, J. Tomasi, M. Cossi, N. Rega, J.M. Millam, M. Klene, J.E. Knox, J.B. Cross, V. Bakken, C. Adamo, J. Jaramillo, R. Gomperts, R.E. Stratmann, O. Yazyev, A.J. Austin, R. Cammi, C. Pomelli, J.W. Ochterski, R.L. Martin, K. Morokuma, V.G. Zakrzewski, G.A. Voth, P. Salvador, J.J. Dannenberg, S. Dapprich, A.D. Daniels, Ö. Farkas, J.B. Foresman, J. Cioslowski, J.V. Ortiz and D.J. Fox, Gaussian 09, Revision A.1, Gaussian Inc., Wallingford CT (2009).
33. H. Kruse, L. Goerigk and S. Grimme, *J. Org. Chem.*, **77**, 10824 (2012); https://doi.org/10.1021/jo302156p
34. N.M. O'Boyle, A.L. Tenderholt and K.M. Langner, *J. Comput. Chem.*, **29**, 839 (2008); https://doi.org/10.1002/jcc.20823
35. L. Skripnikov, Chemissian version 23 (2014); http://www.chemissian.com
36. R. Syed, M. Danish, S. Shakil and M. Haneef, *EXCLI J.*, **12**, 831 (2013).
37. A.H. Abdullah, N.S. Ibrahim, F.K. Algethami, A.H.M. Elwahy, I.A. Abdelhamid and M.E. Salem, *J. Mol. Struct.*, **1302**, 137506 (2024); https://doi.org/10.1016/j.molstruc.2024.137506
38. S. Shaweta, S. Akhil and G. Utsav, *Ann. Antivirals Antiretrovirals*, **5**, 28 (2021); https://doi.org/10.17352/aaa.000013
39. S. Nayab, A. Alam, N. Ahmad, S.W. Khan, W. Khan, D.F. Shams, M.I.A. Shah, M. Ateeq, S.K. Shah and H. Lee, *ACS Omega*, **8**, 17620 (2023); https://doi.org/10.1021/acsomega.2c08266
40. J. Szklarzewicz, A. Jurowska, M. Hodorowicz, G. Kazek, B. Mordyl, E. Menaszek and J. Sapa, *Transition Met. Chem.*, **46**, 201 (2021); https://doi.org/10.1007/s11243-020-00437-1
41. A. Ahmed and R.A. Lal, *Arab. J. Chem.*, **10**, S901 (2017); https://doi.org/10.1016/j.arabjc.2012.12.026
42. M. Muthuppalani, A.A. Otaibi, S. Balasubramaniyan, S. Manikandan, P. Manimaran, G. Mathubala, A. Manikandan, M. Puttegowda, M.N. Arshad, H.S. Alorfi, A. Khan, A.M. Asiri and M.M. Rahman, *Crystals*, **12**, 326 (2022); https://doi.org/10.3390/cryst12030326
43. K. Savithri and H.D. Revanasiddappa, *Bioinorg. Chem. Appl.*, **2018**, 2452869 (2018); https://doi.org/10.1155/2018/2452869
44. E. Garribba and G. Micera, *J. Chem. Educ.*, **83**, 1229 (2006); https://doi.org/10.1021/ed083p1229
45. B.P. Sharma, J.A. Subin, B.P. Marasini, R. Adhikari, S.K. Pandey and M.L. Sharma, *Heliyon*, **9**, e15239 (2023); https://doi.org/10.1016/j.heliyon.2023.e15239